JOURNAL OF AIRCRAFT
Vol. 34, No. 2, March–April 1997

# Forebody Influence on Rotating Parachute Aerodynamic Properties

Z. Shpund* and D. Levin†
*Technion—Israel Institute of Technology, Haifa 32000, Israel*

**For certain requirements of trajectory flight conditions, some parachute–payload systems are mechanically closely coupled systems and have a small diameter ratio of the canopy to the payload. The effect of decreasing diameter ratio on the aerodynamic performance of the system has been experimentally investigated on cross-type rotating parachutes. The results show a significant decrease in the drag coefficient with decreasing diameter ratios, as the forebody wake interferes with the flow around the parachute. Similarly, with an increase of the forebody's diameter, a decrease in the spin was observed. The diameter ratio also affects the static stability. This effect varies between improved stability for short cord configurations, commonly used for submunitions, to a reduction in stability when the cords are longer. The investigation also included the effects of the canopy aspect ratio, different support systems, and the attachment diameter of the cords to the payload.**

## Nomenclature

$C_{M\text{ref}}$ = restoring moment coefficient, $M/q \times S_{\text{ref}} \times D_{\text{ref}}$, reference point defined in Fig. 1
$C_{\text{NOR}}$ = normal force coefficient, $F_{\text{NOR}}/q \times S_{\text{ref}}$
$C_X$ = axial force coefficient, $F_X/q \times S_{\text{ref}}$
$D_B$ = forebody diameter in Ref. 2
$D_{\text{FB ref}}$ = forebody reference diameter, 25 mm, used for forebody alone measurements
$D_l$ = staggering distance, mm
$D_p$ = effective inflated canopy diameter in Ref. 2, for a cross-type canopy, $\sim 2L/\pi$
$D_{\text{ref}}$ = reference length, $L$
$F_{\text{NOR}}$ = normal force, kgf
$F_X$ = axial force, kgf, Fig. 1
$L$ = parachute canopy lobe length, m
$l$ = parachute cords length, m
$M$ = restoring moment, kgf m
$P$ = measured spin rate, rpm
$q$ = dynamic pressure, kg/cm$^2$, $0.5\rho V^2$
$Re$ = Reynolds number per meter $\rho V/\mu$
$S_{\text{ref}}$ = reference area, 1125 cm$^2$
$V$ = velocity, m/s
$W$ = parachute canopy lobe width, m
$W/L$ = parachute canopy lobe aspect ratio
$X_{\text{cp}}$ = c.p. location relative to point of reference, Fig. 1
$\alpha$ = angle of attack, deg
$\mu$ = coefficient of viscosity kg/m s
$\rho$ = air density, kg/m$^3$

## Introduction

PARACHUTES are widely used to attain desired flight conditions (i.e., trajectory angle, velocity, etc.), to influence the payload dynamic behavior, and to induce spin when required to submunitions or other weapon systems. Experience shows that the ratio between the payload diameter and the parachute canopy highly influences the dynamic behavior of the parachute–payload system.

Parachutes used for recovery, having the main role of supplying high drag, and thus, low velocities of descent, have a large canopy diameter compared to the payload dimension. For these systems a low influence of the canopy–payload dimensional ratio on the system aerodynamic characteristics is expected, as the contribution of the payload's aerodynamic properties to the system's aerodynamic characteristics is negligible, especially to the drag coefficient, which is in the focus of interest in that case.

For pilot parachutes, or parachutes designed to shape the trajectory to desired flight conditions (i.e., trajectory angle and velocity), or affect the aerodynamic behavior of the descending payload, the dimensional ratio between the forebody (usually of the payload) and the canopy is smaller than 4 and may decrease to 2 in some systems (Dynamit-Nobel AT-2 Anti-Armor land mine). For these configurations, the contribution of the forebody to the aerodynamic coefficients of the combined configuration is more significant. This contribution is expected to show up in the longitudinal coefficients as well as on the drag coefficient. One of the first published works on this subject was carried out by Niccum et al.,[1] who tested cubical forebodies decelerated by nonrotating cross-type parachutes (some of them erratically rotating). The main scope of their research was the investigation of the aerodynamics of large decelerated payloads (military supplies, etc.) and pilot parachutes. In Ref. 1, the smallest ratio between the forebody characteristic dimension and the reference dimension of the canopy ($L$-lobe length) was 3.6 (corresponding to 0.278 according to the definition in Ref. 1). The main conclusions from this work were that there was only negligible influence on the lateral aerodynamic characteristics and a reduction of 10% of the drag of the combined system was observed compared to larger dimensional ratio configurations.

Reference 2 provides a database concerning the parachute drag loss caused by the forebody wake for canopy diameter to forebody ratio varying from $D_p/D_B = 1.0$ to 3.0. The data presented deal with nonrotating parachutes, mainly drogue (pilot) chutes, operating at high Mach numbers and high altitudes (like the Apollo chute, etc.), and recommends that a certain distance between the forebody and the canopy should be kept to avoid inflation failures and drag loss (six forebody rule). This recommendation is unacceptable for rotating systems or when minimum weight and package volume are required.

A review of other publications, similar to Ref. 3, shows no other investigation of the effect of the forebody size on the

Presented as Paper 95-1555 at the AIAA 13th Aerodynamic Decelerator Systems Technology Conference, Clearwater, FL, May 15–19, 1995; received Aug. 30, 1995; revision received July 21, 1996; accepted for publication Nov. 12, 1996. 

*Research Engineer, Department of Aerospace Engineering.
†Senior Research Associate, Department of Aerospace Engineering.

aerodynamic behavior of a parachute–payload system. Such data may exist in classified reports.

In the current work, an attempt was made to investigate the aerodynamic interference between the payload and the parachute, for rotating and nonrotating systems.

Numeric trajectory system simulation results[4] and wind-tunnel test results[5] show two different modes of motion of the combined system: a unified system motion where the parachute and the forebody perform a rigid body motion, and a second mode, where there is a relative motion between the forebody and the parachute. These two modes of motion required two different measuring sets: a double support system simulating the rigid body motion, and a single forward support system, allowing internal motion between the forebody and the parachute canopy.

## Test Setup and Instrumentation

### Wind Tunnel

The experiments were conducted at the Technion—Israel Institute of Technology, aerodynamic laboratories in the open-loop subsonic wind tunnel, which has a maximal velocity of 32 m/s and a cross section of $1 \times 1$ m$^2$. All of the tests were carried out at a nominal velocity of 20 m/s ($Re = 1.4 \times 10^6$/m).

### Support System and Balances

Two support systems were used, as presented in Fig. 1. A single main balance for the single-support system, and a main and a secondary balance for the double-support system.

The main balance was assembled in the forward strut, which included the attachment to the forebody. For both support systems, the main balance was a six-component, 16-mm-diam sting balance. The secondary balance was mounted in a horizontal position to the rear strut, and supported the parachute model canopy. This balance was a 8-mm-diam, five-component balance.

The support system was attached to the turning floor of the wind-tunnel test section, enabling controlled movement of the whole setup in the pitch plane.

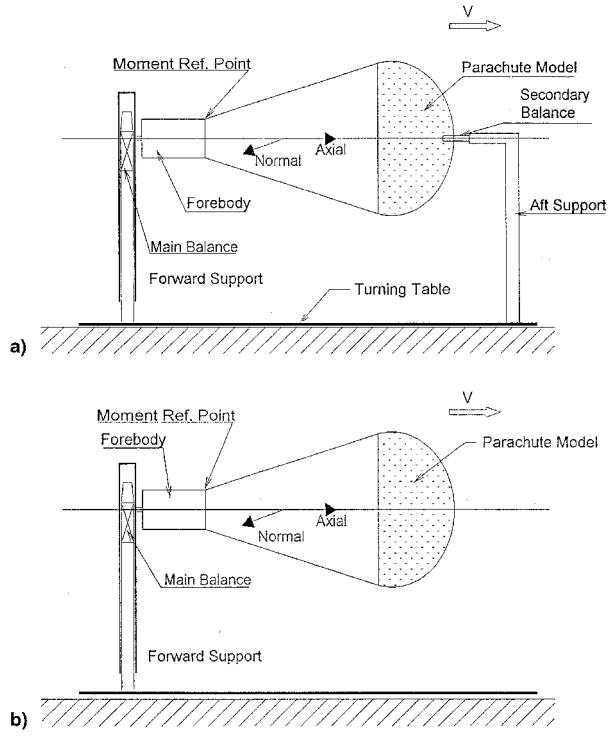


**Fig. 1 Support system setup: a) double and b) single support systems.**

### Forebody

The payload was simulated by a cylindrical forebody. The front end of the forebody was attached to the front strut, and the parachute line-staggering mechanism was attached to the forebody's rear end. The whole system (Fig. 2) was designed to rotate freely around an axis perpendicular to the front strut. The spinning rate was measured by an electro-optical device attached to the static part of the forebody.

The basic diameter of the forebody's cylindrical part was 25 mm. Cylindrical adapters rigidly attached to the forebody, enabling an increase of the diameter of the forebody up to 200 mm, in steps of 25 mm, as described in Fig. 2.

The parachute staggering control device at the rear end of the forebody consisted of two wheels having a diameter of 75 mm. On the circumference of each of the wheels there were four points for the attachment of the parachute lines. Each one of the lines, from each canopy lobe, was attached to one of the wheels (Fig. 2). The two wheels were designed in such a way that when attached to each other, they described a circular attachment, equally divided into eight. In this position, the staggering distance of the parachute line was set to zero. As the two wheels were separated in the $X$ direction (Fig. 2), the line staggering was increased. The maximum staggering distance that could be achieved was 120 mm.

Using adapters, the line attachment diameter could be changed according to the forebody diameter in 25-mm steps from 75 to 200 mm (Fig. 2).

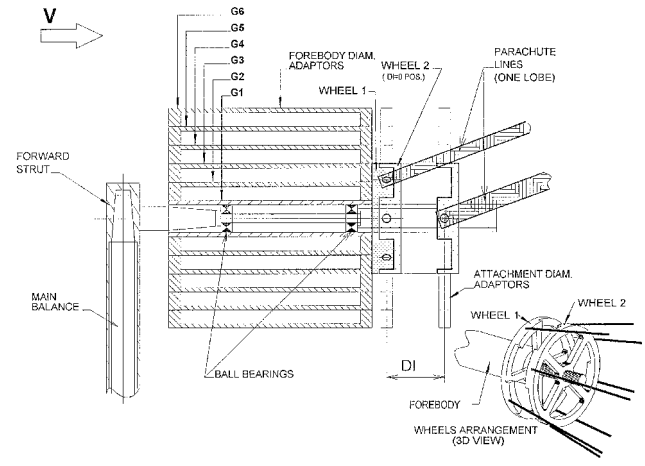


**Fig. 2 Forebody mechanism, general description.**

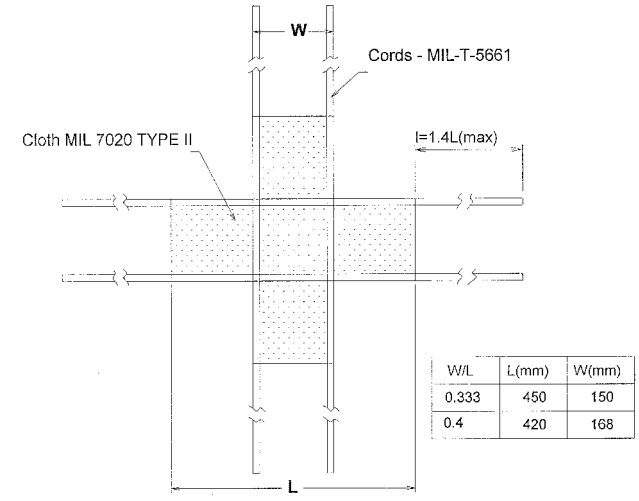


| W/L | L(mm) | W(mm) |
|---|---|---|
| 0.333 | 450 | 150 |
| 0.4 | 420 | 168 |

**Fig. 3 Parachute model details.**

**Table 1 Parameters of the tests**

| Tested parameter | Configuration | Values | Remarks |
|---|---|---|---|
| Forebody diameter | $G1-G6$ | 25 to 150 mm in steps of 25 mm | Simulation of a decelerated cylindrical payload |
| | $G7$ | 200 mm | —— |
| Line staggering, mm | All configurations | $D_l$ = 0, 20, 40 mm | Spin inducement |
| Line length | All configurations | $l/L$ = 0.7, 1.0 | —— |
| Canopy $W/L$ | Main | 0.333, 0.4 | —— |
| Support mode | Double | —— | Simulation of rigid body oscillation |
| | Single | —— | Simulation of relative oscillation |

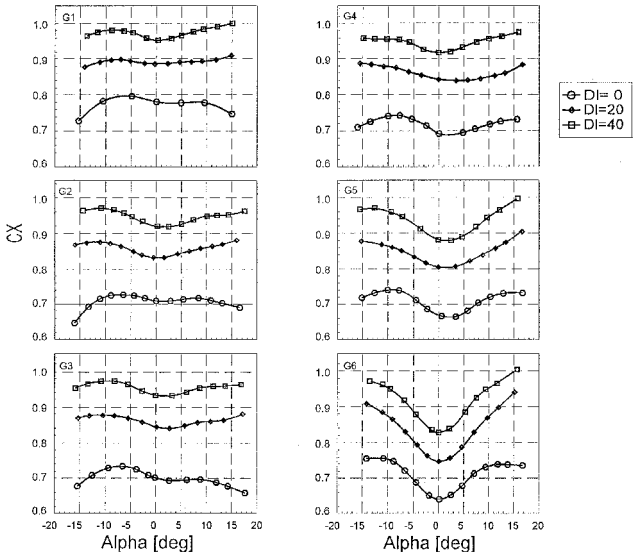


**Fig. 4 Axial force vs α, typical results. Configuration: double support; $l/L$ = 1.0 and $W/L$ = 0.333.**

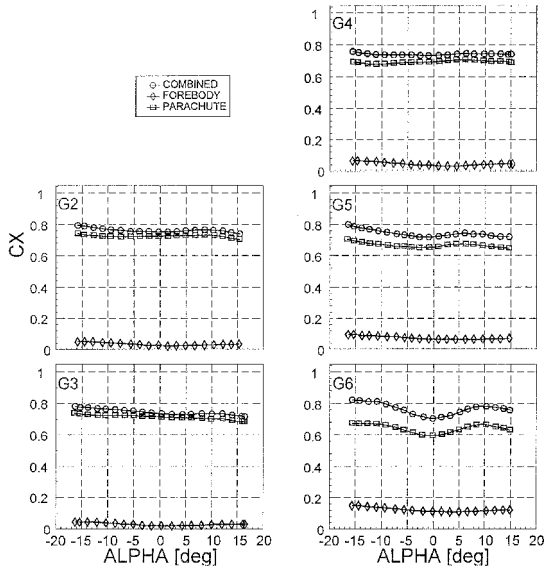


**Fig. 5 Axial force coefficient vs α, deduction of canopy drag contribution. Configuration: single support; $l/L$ = 1.0, $W/L$ = 0.333, and $D_l$ = 0.**

### Parachute model

The cross-type parachute models used had lobe ratios of $W/L$ = 0.333 and 0.4. The geometric details of the canopies and the materials are described in Fig. 3. The line length ratio $l/L$ could be changed from 0.6 to 1.2. However, only length ratios of 0.7 and 1.0 were used.

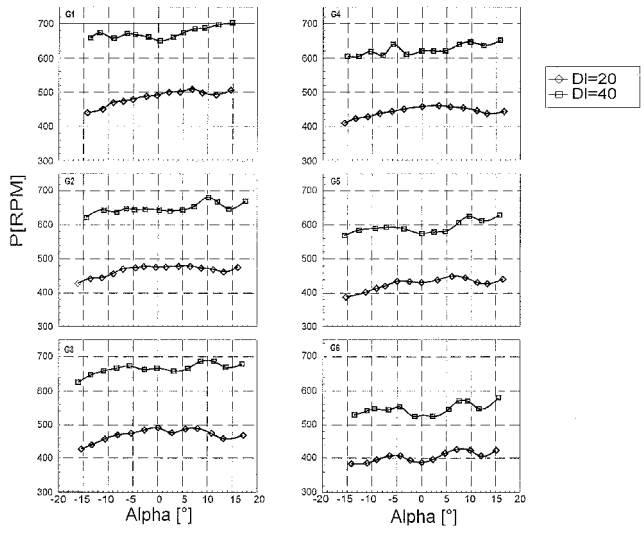


**Fig. 6 $P$ vs α, typical results. Configuration: double support; $l/L$ = 1.0 and $W/L$ = 0.333.**

## Tested Parameters and Results

### Parameters

The main scope of this test series was to investigate the influence of the forebody (simulating the payload) diameter on aerodynamic performance of the combined system. Two support setups (double and single) and two parachute canopy configurations were tested, as detailed in Table 1.

A total of 90 runs with different configurations were performed. The aerodynamic parameters of the forebodies without a parachute model were measured as well, so that the canopy contribution to the combined system could be derived.

The test series was divided into three main groups: 1) $W/L$ = 0.333, main configuration with double and single supports, 2) $W/L$ = 0.4, canopy configuration influence; and 3) enlarged line attachment.

### Results

In each of the runs the axial force, the normal force, the restoring moment, and the spin rate (for rotating configurations) were measured.

A typical set of $C_X$ as a function of the angle of attack, for a double-supported system, is presented in Fig. 4. In Fig. 5, results for a single-supported configuration are presented, including measurement results for the forebody by its axial force. Subtracting the axial force of the forebody alone from the axial force of each specific system enabled the estimation of the canopy drag.

Typical spin rates as functions of angle of attack are presented in Fig. 6.

The $X_{cp}/D_{ref}$ was determined from the gradient of $C_{Mref}$ vs $C_{NOR}$, using a linear regression scheme. Typical results for a $W/L$ = 0.333 canopy configuration, double-support setup, and a staggering distance of 40 mm are presented in Fig. 7.

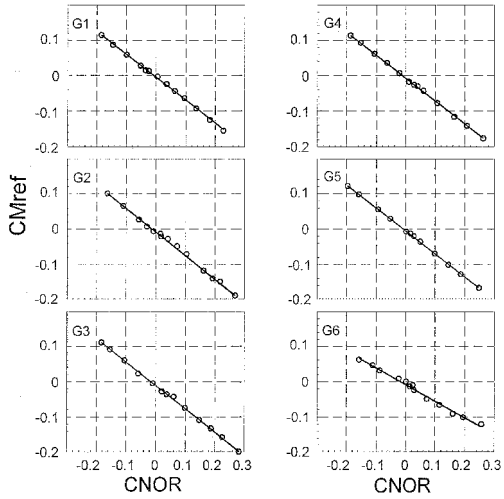


**Fig. 7 Restoring moment as a function of the normal force coefficient, typical results. Configuration: double support; $W/L$ = 0.333, $l/L$ = 1.0, and $D_t$ = 40 mm.**

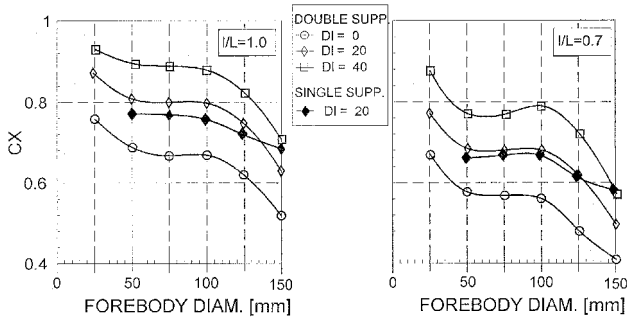


**Fig. 8 Axial force coefficient at α = 0 deg as a function of the forebody diameter for different line length and support system. Configuration: $W/L$ = 0.333.**

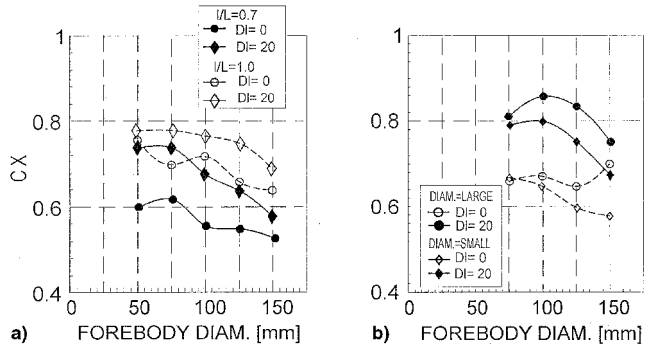


**Fig. 9 Axial force coefficient at α = 0 deg as a function of the forebody diameter: a) $W/L$ = 0.4 canopy configuration and b) attachment diameter effect. Configuration: double support.**

The main results of the forebody effect on the aerodynamic characteristics are presented for zero angle-of-attack conditions as stable parachute–payload systems, operate mainly at α = 0 deg.

The axial force coefficient variation with forebody diameter (at α = 0 deg), is presented in Figs. 8 and 9. The influence of the line lengths and of the support systems (single and double support), is presented in Fig. 8. The axial force variation with the forebody diameter for a canopy of $W/L$ = 0.4 is shown in Fig. 9a, while the effects of the attachment diameter of the parachute cords' length is presented in Fig. 9b. It should be noted that a LARGE attachment diameter defines an attachment diameter equivalent to the forebody diameter (applicable for forebody configurations with $D_{FB} > 75$ mm), and SMALL defines a constant 75-mm attachment diameter independent of the forebody diameter.

A comparison between the axial force results obtained in this research to data presented in Ref. 2 is presented in Fig. 10 for the nonrotating configurations.

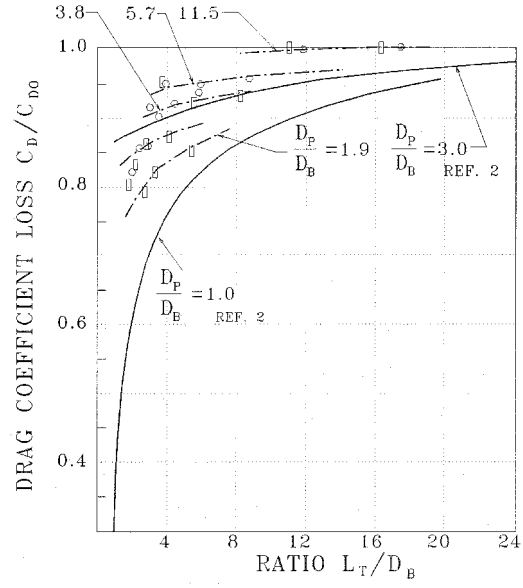


**Fig. 10 Comparison of results from current research to data from Ref. 2.**

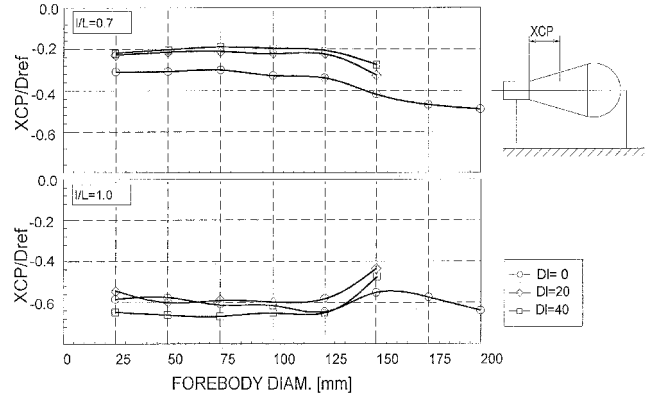


**Fig. 11 Forebody diameter effect on $X_{cp}$ location. Configuration: double support and $W/L$ = 0.333.**

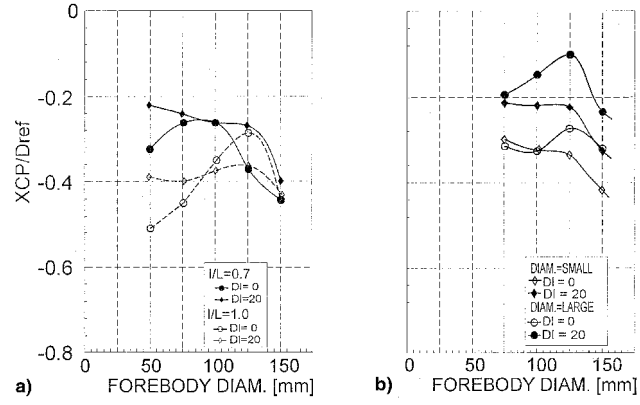


**Fig. 12 Forebody diameter effect on $X_{cp}$ location: a) $W/L$ = 0.4 canopy geometry effect and b) attachment diameter effect. Configuration: double support.**

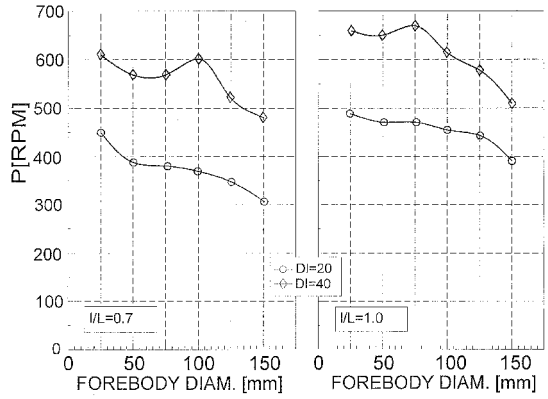


**Fig. 13 Forebody effect on the system spin rate (basic configuration). Configuration: double support and *W/L* = 0.333.**

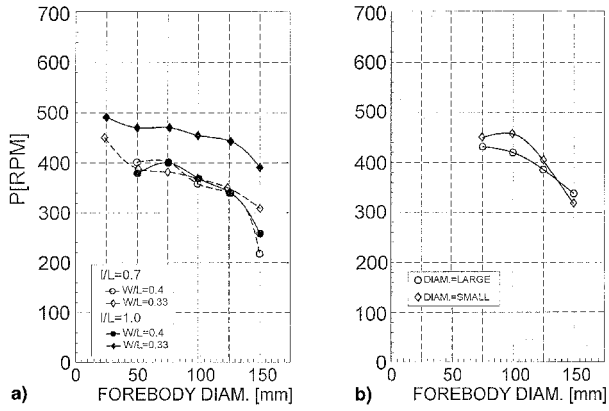


**Fig. 14 Forebody effect on the system spin rate: a) *W/L* = 0.4 canopy geometry effect and b) attachment diameter effect. Configuration: double support and $D_t$ = 20 mm.**

The c.p. location at $\alpha = 0$ deg was also drawn as a function of the forebody diameter, for the various configurations (Figs. 11 and 12).

As the angle of attack has a relatively low influence on the steady-state spin rate developed by the rotating parachute (Fig. 6), for the investigation of the forebody influence on the spin rate, the steady-state spin rate at $\alpha = 0$ deg was drawn (Figs. 13 and 14).

## Discussion

### Axial Force

The axial force characteristic is the most important design property of a decelerating device. For all of the configurations tested a growing deficiency in the drag characteristics close to $\alpha = 0$ deg was observed when the forebody diameter was increased as shown in Fig. 4. This decrease in the system overall drag coefficient of 20% or more, has a significant impact on the design parameters to be considered for the steady-state conditions of a given system.

To explain the reason for this behavior, several runs were carried out with the forebody alone. The results are presented in Fig. 5. The axial force coefficient of the forebody increases as the forebody diameter increases because the same reference diameter ($D_{FB,ref}$) was used for all of the forebodies. The axial force coefficient, however, remains unaffected with the changes of the angle of attack. Tests carried out for configurations having small diameter forebodies show a small dependency of the axial force coefficient on the angle of attack, leading to the conclusion that the decrease in the axial force coefficient at low angles of attack, for large forebody diameters, results from the interference between the two bodies. At low angles of attack, the forebody shadows the airflow to the inflated canopy, thus reducing the mean dynamic pressure acting on the canopy. As the angle of attack is increased, this obstacle is removed, the canopy drag contribution increases, and the drag of the combined system increases.

Proof to this argument can be found when the behavior of the drag deficiency for a single-supported system is examined (Fig. 5). For this setup, the deficiency depth of the axial force coefficient is smaller, but wider, as a function of the angle of attack.

For this support configuration the canopy is free to pitch, with no constraint on its position, but for the aerodynamic forces acting on it. As the forebody moves in the $\alpha$ plane, the canopy remains in its wake in a position dictated by the resultant of the aerodynamic loading on the canopy, and the forces exerted by the parachute cords.

A comparison of the results from the current research to corresponding configurations to Ref. 2 (i.e., nonrotating configurations), is presented in Fig. 10. In the current research, the $D_p/D_B$ ratio varied from ~2 to 11.5, corresponding to forebody diameters varying from 150 to 25 mm, according to the definitions in Ref. 2. It can be seen that there is a good agreement between the current results to the data presented in Ref. 2. All of the configurations having $D_p/D_B < 3$ are within the encompassing lines from Ref. 2. The other configurations, characterized by larger $D_p/D_B$, are above the line, but not very far from it, according to the nonlinear behavior of the parameters already predicted by the encompassing lines.

The spin influence is to increase the drag deficiency close to $\alpha = 0$ deg as spin increases the axial force (as presented in Ref. 6), that is also experienced in the current research. Moreover, the increase in the axial force because of spin increase is almost unaffected by the increase of the forebody diameter.

The axial force deficiency depth obtained with forebody *G*6 ($D_{FB}$ = 150 mm), various canopies, and attachments tested, is shown in Table 2.

It appears that an average decrease of almost 18–20% in the axial force occurs for the *G*6 forebody, which is in good agreement with the data provided in Ref. 2. A larger decrease in axial coefficient happens for the shorter line models (*l/L* = 0.7) and it reaches a minimum of almost a 25% decrease for the *W/L* = 0.4 configuration.

The influence of the forebody diameter can be seen in Fig. 8. In general, a decrease of the axial force is experienced as the forebody diameter is increased. The decrease in the axial force is not monotonic with the increase of the forebody diameter. There is a decrease from $D_{FB}$ = 25 to 50 mm, then the axial force remains almost steady until about $D_{FB}$ = 100 mm, and after that it decreases monotonically for $D_{FB} > 100$. This behavior repeats itself for *l/L* = 0.7 and 1.0, and for various line-staggering ratios.

**Table 2 Relative decrease of the axial force coefficient for tested configurations**

| Configuration | $D_t$ | $C_{X[\alpha=0\ deg]}$ | $C_{X[\alpha=15\ deg]}$ | $\frac{C_{X[\alpha=0\ deg]}}{C_{X[\alpha=15\ deg]}}$ |
|---|---|---|---|---|
| *l/L* = 0.7 | 0 | 0.58 | 0.72 | 0.81 |
| *W/L* = 0.333 | 20 | 0.68 | 0.84 | 0.81 |
| Double support | 40 | 0.77 | 0.93 | 0.83 |
| *l/L* = 1.0 | 0 | 0.63 | 0.76 | 0.83 |
| *W/L* = 0.333 | 20 | 0.74 | 0.91 | 0.81 |
| Double support | 40 | 0.83 | 0.98 | 0.84 |
| *l/L* = 0.7 | —— | —— | —— | —— |
| *W/L* = 0.4 | 0 | 0.52 | 0.68 | 0.76 |
| Double support | 20 | 0.57 | 0.74 | 0.77 |
| *l/L* = 1.0 | —— | —— | —— | —— |
| *W/L* = 0.4 | 0 | 0.68 | 0.8 | 0.85 |
| Double support | 20 | 0.7 | 0.85 | 0.82 |
| Large attachment | —— | —— | —— | —— |
| *W/L* = 0.333 | 0 | 0.7 | 0.85 | 0.82 |
| Double support | 20 | 0.76 | 0.9 | 0.844 |

The difference in the axial force results, measured by a double- and a single-support system, is also presented in Fig. 8. This difference in the axial force is explained by the difference between the two supporting configurations. In general, the behavior of the two axial forces, as the forebody diameter is increased, is almost identical. The difference in the magnitudes may be related to the different shape of the canopy obtained by the difference in the support systems.

The axial force decrease as a function of growing forebody diameter, as shown in Fig. 9a for a canopy with $W/L = 0.4$, is similar to that obtained for the canopy $W/L = 0.333$.

The effects of the attachment diameter variations are presented in Fig. 9b. An increase in the axial force is observed compared to a smaller attachment diameter. The reason for this increase in the axial force is related to the increase of the canopy-projected area as the attachment diameter is increased.

### Lateral Stability

An aerodynamic configuration is statically stable when the c.p. is located behind the center of gravity c.g. The location of $X_{cp}$ relative to the c.g. (the reference point, Fig. 1) for the main tested configuration is shown in Fig. 11.

In general, all of the tested configurations are statically stable. The c.p. location is almost unaffected as the forebody diameter is increased to $D_{FB} = 125$ mm. For larger diameters, an increase of stability ($X_{cp}$ becomes more negative) was observed for the $l/L = 0.7$ configurations, and a decrease in stability ($X_{cp}$ becomes less negative) for the $l/L = 1.0$ configurations.

To further test this trend, two more tests were carried for the nonrotating configurations ($D_l = 0$). The results of these tests show a further increase in the lateral stability for the short-corded configuration ($l/L = 0.7$), whereas for the longer line configuration the trend is not clear.

The stability of a system having a single support cannot be measured or evaluated, as the canopy axis tends to remain parallel to the flow, although the forebody is rotated in the $\alpha$ plane.

For the $W/L = 0.4$ canopy, the stability results are presented in Fig. 12a. The data show a slight increase of stability for the short-cord configurations ($l/L = 0.7$) as the forebody diameter is increased. For the longer lines ($l/L = 1.0$) the trend is not clear.

The effect of the attachment diameter on the position of $X_{cp}$ is presented in Fig. 12b. For both configurations, nonrotating ($D_l = 0$) and rotating ($D_l = 20$), a decrease in stability is obtained when the attachment diameter is increased. This decrease in stability grows ($X_{cp}$ becomes less negative) with increasing forebody diameter.

### Rate of Spin

Previous works[5,6] show a low dependency of the spin rate on the angle of attack. The current measurements show similar results (Fig. 7). The main point of interest for an aerodynamically stable system is the spin rate at low angles of attack ($\alpha \sim 0$ deg). The forebody effect on the spin rate is shown in Fig. 13 (double support, $W/L = 0.333$). One can see a monotonic decrease of the spin rate as the forebody diameter is increased. In general, for both supports, a decrease of 20% was measured for the configurations tested ($l/L = 0.7$ and 1.0). A decrease of the spin rate as a result of shorter cords has been previously reported.[5]

A similar behavior of the forebody influence on the spin rate was observed for $W/L = 0.4$, as shown in Fig. 14a. In this case, the reduction in spin rate is more significant than for $W/L = 0.333$, and reaches almost 33–45%.

An increase of the attachment diameter is one of the ways to avoid cords' winding tendency, for high spin-up systems. Intuitively, an increase of the system spin rate is expected when the attachment diameter is increased. However, the spin variation presented in Fig. 14b shows that the attachment diameter has a negligible effect on the spin rate of the combined system.

## Conclusions

An experimental study investigating the effect of the forebody size on the aerodynamic characteristics of a closely coupled parachute–payload system was conducted in a low-speed subsonic wind tunnel.

The primary model consisted of a cross-type parachute having a $W/L = 0.333$ with a double-support system, simulating a rigid body mode of motion. The payload was a cylinder with variable diameter. The test parameters included the line ratio, the staggering ratio, payload diameter, and the diameter of the attachment device of the suspension lines. Some tests were also conducted with a single-support system and with a canopy having $W/L = 0.4$.

It was found that the increase of the forebody diameter had a major influence on the drag characteristics. As the forebody diameter was increased to 33% of the canopy characteristic dimension $L$, a decrease of 20–25% was experienced in the axial force for low angles of attack, caused by aerodynamic interference between the forebody and the parachute canopy. These results are in good agreement with previously published data[2] for nonrotating parachute configurations.

This decrease was measured between $\alpha = -15$ and $+17$ deg, attaining a minimum at $\alpha = 0$ deg for the double-support system. For the single-support system, the interference domain was found to be larger ($\alpha = \pm 21$ deg) because of the tendency of the canopy to remain in the forebody's wake as the angle of attack was increased.

As the forebody diameter was increased, a degradation in the lateral stability of the system was found for configurations with long cords ($l/L = 1.0$), whereas for short cords ($l/L = 0.7$) the stability was increased.

The spin of the canopy did not affect the decrease in the axial force at low angles of attack, but the increase of the forebody diameter reduced the steady-state spin rate by almost 25% for $W/L = 0.333$ parachutes, and almost 33% for parachutes with $W/L = 0.4$.

An increase of the attachment diameter, which is a way to avoid cords winding (choking) of spinning parachutes, did not affect the drag and spin rate of the parachutes, but a decrease in the lateral stability was experienced.

## References

[1]Niccum, R. J., Haak, E. L., and Gutenkauf, R., "Drag and Stability of Cross Type Parachutes," Univ. of Minnesota, FDL-TDR-64-155, Minneapolis, MN, 1964.

[2]Knacke, T. W., *Parachute Recovery Systems—Design Manual*, 1st ed., Para Publishing, Santa Barbara, CA, 1992.

[3]"Recovery Systems Design Guide," Air Force Flight Dynamics Lab., TR-78-151, Dec. 1978.

[4]Doherr, K.-F., and Schiling, H., "Nine-Degree-of-Freedom Simulation of Rotating Parachute Systems," *Journal of Aircraft*, Vol. 29, No. 5, 1992, pp. 774–781.

[5]Levin, D., and Shpund, Z., "Dynamic Investigation of the Angular Motion of a Rotating Body-Parachute System," *Journal of Aircraft*, Vol. 32, No. 1, 1995, pp. 93–99.

[6]Shpund, Z., and Levin, D., "Measurement of the Static and Dynamic Aerodynamic Coefficients of a Cross Type Parachute in Subsonic Flow," AIAA Paper 91-0870, April 1991.